

AD-A178 139

A SEARCH FOR PRECURSOR ACTIVITY ASSOCIATED WITH CORONAL
MASS EJECTIONS US. (U) NAVAL RESEARCH LAB WASHINGTON DC
J T KARPEN 31 DEC 85 AFGL-TR-86-0056 MIPR-FV7121850006

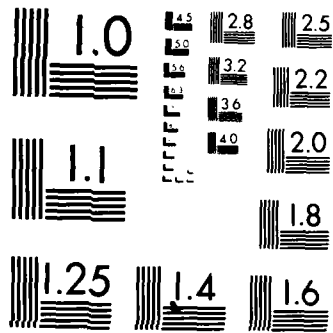
1/1

UNCLASSIFIED

F/G 3/2

NL





MICROCOPY RESOLUTION TEST CHART
NATIONAL BUREAU OF STANDARDS-1963-A

12

AFGL-TR-86-0056

A Search for Precursor Activity Associated With Coronal Mass Ejections,
Using White-Light Coronagraph Observations Obtained With the SOLWIND
Instrument on Board the Air Force P78-1 Satellite

Judith T. Karpen

Naval Research Laboratory
4555 Overlook Avenue, S.W.
Washington, DC 20375-5000

31 December 1985

Final Report
15 September 1984 - 31 December 1985

APPROVED FOR PUBLIC RELEASE; DISTRIBUTION UNLIMITED

AIR FORCE GEOPHYSICS LABORATORY
AIR FORCE SYSTEMS COMMAND
UNITED STATES AIR FORCE
HANSCOM AIR FORCE BASE, MASSACHUSETTS 01731

DTIC
ELECTE
JUL 25 1986
S D
D


AD-A170 139

DTIC FILE COPY


36 7 28 019

This technical report has been reviewed and is approved for publication.


RICHARD C. ALTROCK
Contract Manager


STEPHEN L. KEIL
Chief, Solar Research Branch

FOR THE COMMANDER


RITA C. SAGALYN, Director
Space Physics Division

This report has been reviewed by the ESD Public Affairs Office (PA) and is releasable to the National Technical Information Service (NTIS).

Qualified requestors may obtain additional copies from the Defense Technical Information Center. All others should apply to the National Technical Information Service.

If your address has changed, or if you wish to be removed from the mailing list, or if the addressee is no longer employed by your organization, please notify AFGL/DAA, Hanscom AFB, MA 01731. This will assist us in maintaining a current mailing list.

Do not return copies of this report unless contractual obligations or notices on a specific document requires that it be returned.

A170139

REPORT DOCUMENTATION PAGE

1a REPORT SECURITY CLASSIFICATION UNCLASSIFIED		1b RESTRICTIVE MARKINGS	
2a SECURITY CLASSIFICATION AUTHORITY		3 DISTRIBUTION/AVAILABILITY OF REPORT Approved for public release; distribution unlimited	
2b DECLASSIFICATION/DOWNGRADING SCHEDULE		4 PERFORMING ORGANIZATION REPORT NUMBER(S)	
4 PERFORMING ORGANIZATION REPORT NUMBER(S)		5 MONITORING ORGANIZATION REPORT NUMBER(S) AFGL-TR-86-0056	
6a NAME OF PERFORMING ORGANIZATION Naval Research Laboratory	6b OFFICE SYMBOL (if applicable) Code 4175K	7a NAME OF MONITORING ORGANIZATION Air Force Geophysics Laboratory	
6c ADDRESS (City, State, and ZIP Code) 4555 Overlook Avenue, S.W. Washington, DC 20375-5000		7b ADDRESS (City, State, and ZIP Code) Hanscom AFB Massachusetts 01731	
8a NAME OF FUNDING/SPONSORING ORGANIZATION AFGL	8b OFFICE SYMBOL (if applicable) PHS	9 PROCUREMENT INSTRUMENT IDENTIFICATION NUMBER MIPR #FY71218500006	
8c ADDRESS (City, State, and ZIP Code) Hanscom AFB, MA 01731		10 SOURCE OF FUNDING NUMBERS	
		PROGRAM ELEMENT NO. 61102F	PROJECT NO. 2311
		TASK NO. G3	WORK UNIT ACCESSION NO. DF
11 TITLE (Include Security Classification) A Search for Precursor Activity Associated with Coronal Mass Ejections, Using White-light Coronagraph Observations Obtained With the SOLWIND Instrument on Board the Air Force P78-1 Satellite (UNCLASSIFIED)			
12 PERSONAL AUTHOR(S) Karpen, Judith T.			
13a TYPE OF REPORT Final	13b TIME COVERED FROM 84/9/15 TO 85/12/31	14 DATE OF REPORT (Year, Month, Day) 85/12/31	15 PAGE COUNT 24
16 SUPPLEMENTARY NOTATION			
17 COSATI CODES		18 SUBJECT TERMS (Continue on reverse if necessary and identify by block number)	
FIELD	GROUP	SUB-GROUP	solar physics - coronal mass ejections - precursors
19 ABSTRACT (Continue on reverse if necessary and identify by block number)			
<p>Large-scale coronal disturbances preceding solar flares or other surface activity and resulting in mass ejection, are perhaps the most intriguing and least understood manifestations of preflare/pre-mass-ejection activity seen to date. The existence of energetic disturbances in the corona significantly before the associated surface events has profound implications for the location and mechanism of preflare energy storage, as well as the evolution and magnitude of the energy release or magnetic disequilibrium characterizing the interval before and during the mass ejection. Jackson and Hildner (1978; JH) studied 18 coronal mass ejections (CMEs) observed with the SKYLAB white-light coronagraph. They found a low-density plateau rimming each event, and denoted this phenomenon a "forerunner." In addition, they concluded that the forerunner material must be set in motion significantly before the onset of the associated CME (cf. Jackson 1981), and could not be explained by mere translation of the overlying coronal plasma. We have performed a</p> <p style="text-align: right;">(Over)</p>			
20 DISTRIBUTION/AVAILABILITY OF ABSTRACT <input checked="" type="checkbox"/> UNCLASSIFIED/UNLIMITED <input type="checkbox"/> SAME AS RPT <input type="checkbox"/> DTIC USERS		21 ABSTRACT SECURITY CLASSIFICATION UNCLASSIFIED	
22a NAME OF RESPONSIBLE INDIVIDUAL Dr. R.C. Altrock		22b TELEPHONE (Include Area Code) (505) 434-1390	22c OFFICE SYMBOL AFGL/PHS

7. systematic search for forerunners using the white-light coronagraph observations obtained with the SOLWIND instrument on board the P78-1 satellite. We selected and analyzed 44 bright, well-observed events, employing selection criteria and analysis methods similar to those used by JH. → In comparing the SOLWIND difference images to the excess mass contours, we find that the 2-sigma contour level used by JH to define the forerunner front is readily apparent in the images. In fact, this level generally outlines the leading edge of the visible event. If the contour plots of the SOLWIND events are made with the same (linear) contour spacing as used by JH, a forerunner plateau is visible in both the CME itself and nearby affected coronal features, e.g., a neighboring streamer that has been pushed aside. If contour levels with power-law spacing similar to the density distribution of the background corona are chosen, however, the forerunner plateau disappears. Therefore, we conclude that the forerunner phenomenon is an integral part of the CME itself and not a manifestation of precursor activity.

TABLE OF CONTENTS

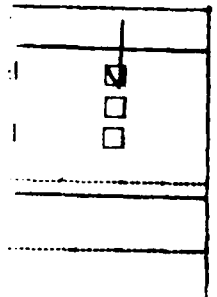
I. Introduction	1
II. Observations and Data Analysis	4
III. Results	9
IV. Discussion	15
Acknowledgements	18
References	18

LIST OF TABLES

1. Properties of the Events Studied	7
-------------------------------------	---

LIST OF FIGURES

1. A white-light difference image of the coronal mass ejection of 1982 July 22, 1720 UT, observed with the SOLWIND coronagraph.	9
2. Isodensity contours of excess column density (in g cm^{-2}) for the 1982 July 22 event at 1720 UT, taken from a portion of the image shown in Figure 1.	10
3. The profile of excess density (in g cm^{-2}) vs distance from the solar surface (in solar radii) for the 1982 July 22 event at 1720 UT, along the radial cut partially shown in Figure 2.	11
4. A white-light difference image of the coronal mass ejection of 1981 February 23, 0245 UT, observed with the SOLWIND coronagraph.	12
5. Same as Figure 2 for the 1981 February 25 event at 0245 UT, taken from a portion of the image shown in Figure 4.	13
6. Same as Figure 3 for the 1981 February 25 event at 0245 UT, for the radial cut partially shown in Figure 5.	13
7. Isodensity contours of excess column density (in g cm^{-2}) for the 1981 February 25 event at 0245 UT taken from a portion of the image shown in Figure 1.	16



Availability Codes	
Dist	AVAILABILITY STATEMENT
A-1	UNCLASSIFIED

I. INTRODUCTION

Coronal mass ejections (CMEs) are expulsions of solar plasma into the corona and beyond. They are associated frequently with energetic surface phenomena, particularly eruptive prominences (Munro et al. 1979). A typical mass ejection travels at 500 km s^{-1} and contains approximately $4 \times 10^{15} \text{ g}$ of excess material (Howard et al. 1985). Although plasma ejections from the Sun were postulated decades ago, the first significant samples of these events were obtained by spaceborne white-light coronagraphs in the early 1970s (e.g., Koomen et al. 1974; Hildner 1977).

Approximately half of the events seen by the HAO coronagraph on SKYLAB assumed the shape of an outwardly moving loop or blob (MacQueen 1980). A more detailed morphological classification of the 77 major CMEs observed during SKYLAB yields approximately 25% loop-type events and 10% filled-bottle events (Munro and Sime 1985). In comparison, a similar morphological study of the nearly 1000 CMEs observed by the SOLWIND white-light coronagraph during 1979-1981 yields a combined total of 28% loop, double-spike, and curved-front events; no category corresponds directly to Munro and Sime's "filled bottle" events, however (see Howard et al. 1985 for definitions of SOLWIND morphological types). These mass ejections probably are not planar loops, but rather resemble three-dimensional bubbles, either hollow or filled with excess mass (Howard et al. 1982; Wagner 1984). In general, the loop and curved-front transients are the most clearly defined CMEs in terms of discerning an outer edge in excess density in the white-light images. Thus, this type of mass ejection provides the best opportunity to determine the state of the corona ahead of the expelled material.

Jackson and Hildner (1978; JH) investigated the morphology of 18 loop-type CMEs in the SKYLAB data set, with particular emphasis on the coronal plasma bordering the primary events. They found a broad rim of excess density (above the 2-sigma level) -- which they denoted a "forerunner" -- around the edges of each transient. The configuration and speed of each forerunner appear similar to those of the underlying CME, so that a nearly constant offset is maintained between the outer boundaries of the forerunner and the transient. JH conclude that the forerunner phenomenon cannot be attributed to a simple translation of coronal material pushed from lower heights ahead of the CME, because the observed density of the forerunner is too low. Two other explanations for the additional density in forerunners are considered: preexisting coronal plasma which is compressed in situ (e.g., Wu et al. 1978; Mouschovias and Poland 1978), or coronal material driven ahead of an impulse which must originate earlier than the transient itself (cf. Jackson 1981). These hypotheses represent fundamentally different physical processes and provide important constraints on models of coronal mass ejections. The forerunner phenomenon, then, might be linked to preflare activity as well as to the coronal response to the energy release (or loss of equilibrium; cf. Low 1981, 1982, 1984; Wolfson and Gould 1985) initiated by certain surface events. The study of forerunners also may benefit flare prediction capabilities, in improving our understanding of preflare activity and its heliospheric repercussions.

For flare-associated mass ejections, there is growing evidence that the CME and the flare are initiated separately (Simnett and Harrison 1985), although there must be a connection between these temporally correlated phenomena. The published information on forerunners is not sufficient to

address these issues fully, however. Since the OSO-7 and SKYLAB era, white-light forerunners have been reported for a few CMEs at most (e.g., Gary et al. 1984). Other solar phenomena have been observed to precede coronal transients spatially or temporally. Weak soft X-ray enhancements have been detected 15 to 30 minutes before the onset of flare activity, but roughly coincident with the projected starting time of mass ejection from the low corona (Harrison et al. 1984; Simnett and Harrison 1985). Type II radio bursts associated with CMEs probably start minutes later than the mass ejection, but frequently travel with much higher velocities and overtake the leading edge of the transient (Gergely 1984). The MHD shocks which are thought to produce Type II bursts (Wild, Smerd, and Weiss 1963; Malitson et al. 1973) and often accompany CMEs (Gosling et al. 1974; Sheeley et al. 1983, 1985) also might account for the excess plasma comprising forerunners (e.g., Dulk et al. 1976; Gary et al. 1984). Doppler scintillation observations of CME-associated interplanetary shocks indicate that the shock front travels faster than the leading edge of the white-light CME, and thus could be responsible for a detectable plasma excess ahead of the ejection itself (Bird et al. 1985; Woo et al. 1985). Further in-depth study of a much greater sample of events is required, however, to establish a connection (if any) between forerunners and other CME-associated activity.

We have performed a systematic search for forerunners in the data obtained with the SOLWIND white-light coronagraph on board the P78-1 satellite (Michels et al. 1980). This data set contains over 1000 CMEs, at present, from which we have selected 44 bright CMEs of the loop and curved-front categories for detailed analysis. We describe the event selection and analysis in Section II. The results of this investigation are presented and

compared with the work of JH and Jackson (1981) in Section III. Based on these results, we conclude that there is no evidence for precursor activity (of the form identified by JH) ahead of the SOLWIND coronal mass ejections. We discuss these conclusions and suggestions for future work in Section IV.

II. OBSERVATIONS AND DATA ANALYSIS

We briefly summarize the instrumental and data-set characteristics, as detailed descriptions of the SOLWIND coronagraph are published elsewhere (Sheeley et al. 1980; Michels et al. 1982). Routine observations of the corona by the SOLWIND instrument began on 28 March 1979 and ended on 13 September 1985. The field of view extends roughly from 2.5 to 10 R_{\odot} , with spatial resolution of 1.25 arcmin. The interval between images is 10 minutes, for the most part, with occasional periods in which images were obtained every 5 minutes during the 1-hour daylight portion of the 93-minute orbit. The duty cycle and intermittent gaps of no coverage are described more thoroughly by Howard et al. (1985). The instrument sensitivity is comparable to that of the SKYLAB coronagraph.

We have reproduced the analysis procedures of JH as closely as possible, given the differences between the SKYLAB and SOLWIND coronagraphs and between the methods used to reduce the initial data from each instrument. In this way, our operational definition of the forerunner phenomenon has been confined to an established standard. JH used the following basic format in their forerunner search. The coronal images obtained by SKYLAB originally were on film. These images were digitized for further processing. Transients are most easily detected using difference images, formed by subtracting a base image from one taken at a later time. The excess brightness images first were

averaged over 5 x 5 neighboring pixels to smooth out excess noise; the spatial resolution thus achieved was 120 by 120 arcsec. The resultant difference images were converted from units of excess brightness to excess column density (cf. Hildner et al. 1975 for details), and contour plots were made. The outer boundary of the forerunner was defined arbitrarily as the $6 \times 10^{-9} \text{ g cm}^{-2}$ contour level of excess column density, which is the 2-sigma level of noise in the difference images. The outer boundary of the forerunners reported by JH actually extended beyond this level, fading eventually into the background. In contrast, the majority of transients in their sample were characterized by a sharp outer edge which occurred approximately at the $50 \times 10^{-9} \text{ g cm}^{-2}$ level. Therefore, JH adopted this contour of excess mass as the working definition of the boundary between the transient and the forerunner. Radial scans through the approximate center of each event also were made, to show the run of excess column density with height above $1.6 R_{\odot}$.

In our survey of the SOLWIND coronagraph data, we used the existing set of difference images on Polaroid film to identify promising events for further scrutiny. For proper registration, the two images used to make a difference image are temporally separated by a multiple of the satellite orbital period. We chose the smallest possible multiple for which a good base image could be obtained, to minimize the distracting influence of long-term changes in the background coronal structure. The digital data were reduced on a VAX 11/730 computer, with an IIS image processing and display system used to determine the radial-cut locations and contouring areas. Each pair of images were calibrated in units of coronal brightness before differencing. As was done by JH, we smoothed the difference images by averaging over 5 x 5 neighboring pixels. The smoothed difference images were displayed for identification of

the radial cut lines and the portion of the image to be contoured. Then, these data were converted to units of excess column density (cf. Poland et al. 1981). To produce contour plots with minimum noise, the data were filtered before contouring using the algorithm of Lee (1981).

Our selection criteria were as follows:

- 1) The event intensity must be average or bright, according to the classification scheme outlined by Howard et al. (1985).
- 2) The morphological type must be a loop, curved front, or complex (as long as criterion #3 is satisfied), according to the classification scheme outlined by Howard et al. (1985).
- 3) The event must have a clearly visible front throughout most, if not all, of the observation period. In all but a few cases, the position of the leading edge at the initial time of observations was less than about $4 R_{\odot}$.
- 4) The outer portions of the event are not obscured by one of the polarizing rings (located at approximately 5 and $8 R_{\odot}$). For events with good coverage (i.e., several images), this criterion was obeyed by discarding those images in which the region ahead of the transient is in one of the polarizing rings. Events for which most or all of the images violate this criterion were not used.

Using these criteria, we selected 44 CMEs for in-depth study. The observation intervals and observed characteristics for these events are listed in Table 1. Two plots were produced for each image: a contour plot of the excess mass density in the region containing the CME, and a plot of the excess density in and ahead of the CME along a radial cut from the Sun's center to approximately $10 R_{\odot}$. The same radial cut was used for all images of each event, and traverses a dense, well-defined portion of the CME.

Table 1. Properties of the Events Studied

Date	Time of First Image (UT)	Number of Images	Speed (km s ⁻¹)	Morphological Type*
1979 April 2	2226	1	150	CF
May 4	0219	3	870	CF
May 8	1028	4	375	CF
May 24	1635	2	1000	L
June 9	1613	2	590	L
July 3	0038	4	580	CF
July 27	0652	6	460	CF
August 14	1306	1	1200	CF
August 16	2246	5	640	L
August 26	0235	9	445	CF
August 26	0235	9	480	L
October 30	1445	10	670	CF
November 1	0656	8	1420	CF
November 15	2239	2	1200	CMPX
November 17	0311	2	890	CF
1980 April 3	0728	3	1100	CF
May 22	2154	8	300	CF
June 12	1237	3	490	CF
June 18	2221	4	520	CF
September 6	0426	4	280	L
September 7	0000	5	700	CF
November 8	0321	3	755	CF
November 17	1122	2	200	CF

Table 1. Properties of the Events Studied (Continued)

Date	Time of First Image (UT)	Number of Images	Speed (km s ⁻¹)	Morphological Type*
1981 January 26	0303	3	1200	CF
February 25	0245	5	715	CF
March 5	0737	4	425	CF
April 10	1135	3	775	CMPX
May 10	0732	5	830	CF
May 10	1229	2	1420	CF
June 27	0928	4	860	CF
August 6	2317	7	245	CF
August 13	2122	5	450	CF
October 18	0330	5	700	CMPX
October 25	0017	5	950	CMPX
November 9	0536	11	490	CF
November 13	0500	5	480	CMPX
November 17	0619	11		CF
November 18	2106	5	900	CF
December 20	0559	5	305	L
1982 January 9	1416	2	840	CF
January 19	0800	10	50	CMPX
July 22	1720	3	1750	CMPX
1984 July 14	0934	10	330	CF

* CF = curved front

L = loop

CMPX = complex

(see Howard et al., 1985)

III. Results

To illustrate the characteristics of the CMEs in our data set, we present in detail the results of our analysis for two of the 44 mass ejections . These CMEs occurred on 1981 February 25 and 1982 July 22. We first observe the 1982 July 22 event at 1720 UT, when the white-light front is already at $3.5 R_{\odot}$ (Figure 1).

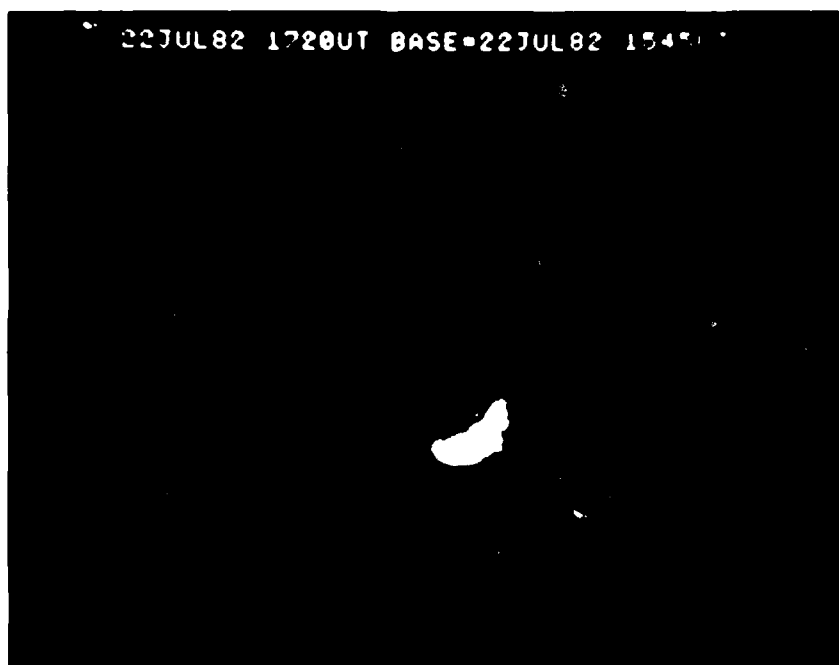


FIGURE 1. A white-light difference image of the coronal mass ejection of 1982 July 22, 1720 UT, observed with the SOLWIND coronagraph. The base image used for differencing was taken at 1545 UT. The field of view of the image extends from the outer edge of the occulting disk, at about $2.6 R_{\odot}$, to $8 R_{\odot}$.

Figure 2 is a plot of isodensity contours for the 1982 July 22 CME. There is little evidence for forerunner activity (as defined by JH) ahead of the CME, although more of a plateau is evident around the sides. The spiky nature of the lowest contour (at $6 \times 10^{-9} \text{ g cm}^{-2}$) is due to the presence of coronal streamers which might have been enhanced in conjunction with the CME.

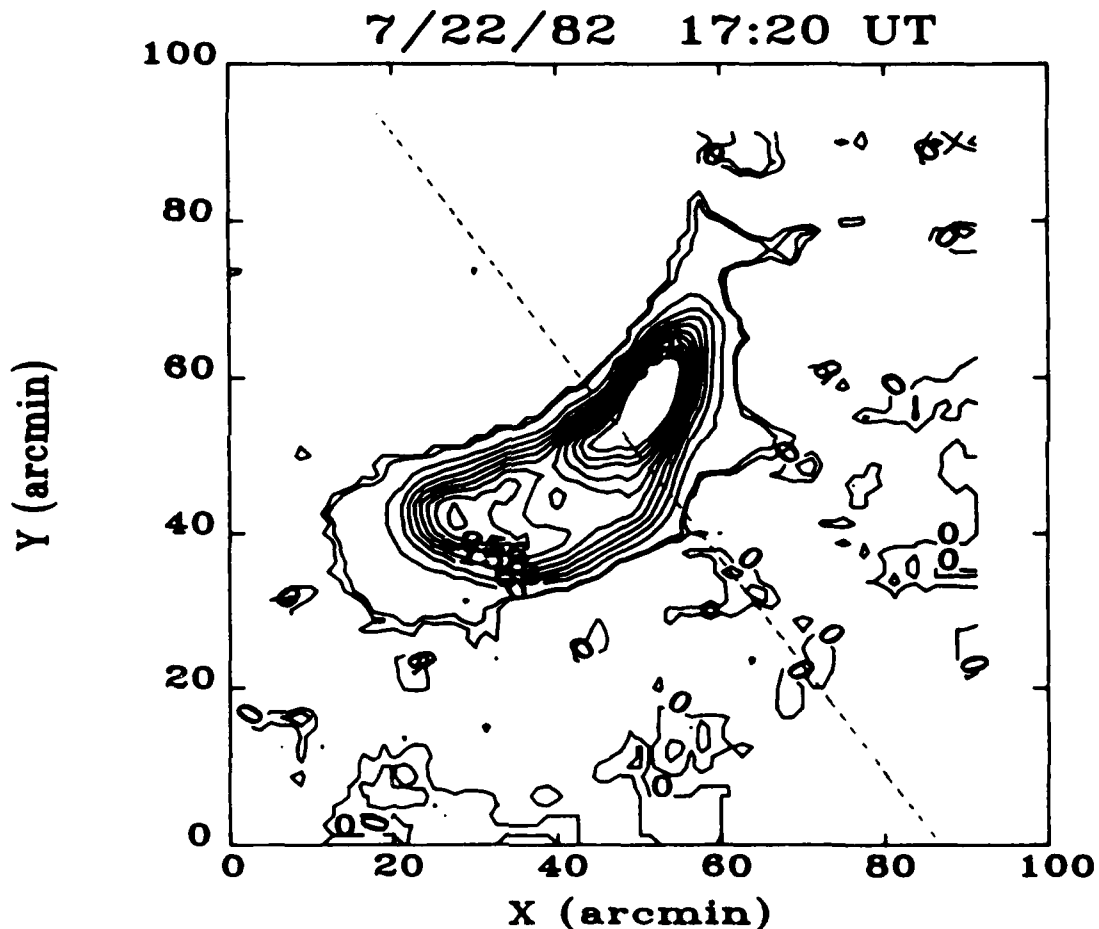


FIGURE 2. Isodensity contours of excess column density (in g cm^{-2}) for the 1982 July 22 event at 1720 UT, taken from a portion of the image shown in Figure 1. The contour levels are drawn at 0, 6, 56, 106, 156, 206, 256, 306, 356, 406, and $456 \times 10^{-9} \text{ g cm}^{-2}$. Values above $456 \times 10^{-9} \text{ g cm}^{-2}$ are not shown. A portion of the radial cut used to produce the density-height plot (Figure 3) is shown by the dotted line through the CME.

The lack of forerunner material also is visible in the radial-cut plot (Figure 3), which depicts a monotonically decreasing excess density profile through the approximate center of the mass ejection.

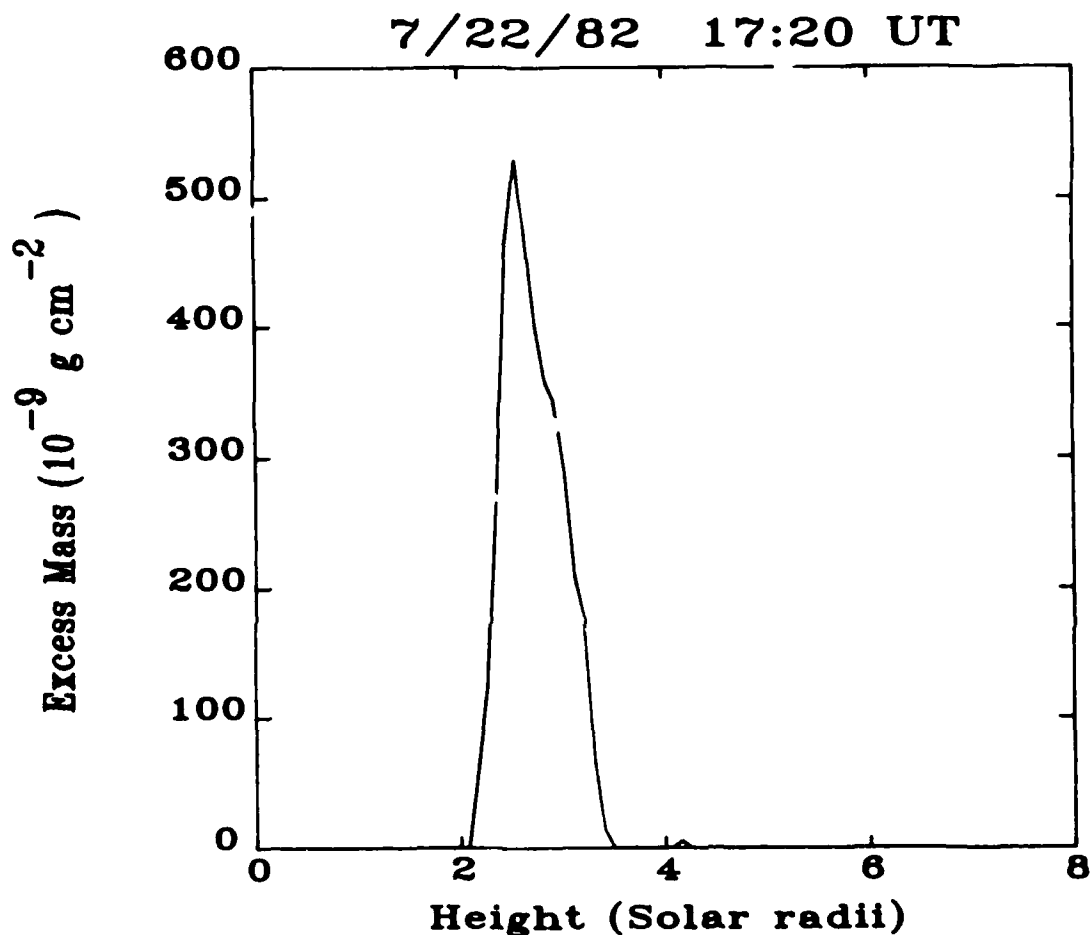


FIGURE 3. The profile of excess density (in g cm^{-2}) vs. distance from the solar surface (in solar radii) for the 1982 July 22 event at 1720 UT, along the radial cut partially shown in Figure 2. The entire radial cut starts at Sun center and ends around $10 R_{\odot}$.

The 1981 February 25 event has a different and more complex appearance. The primary feature, located nearest the center of the image (Figure 4), is the CME, while the narrower feature below and to the right is a streamer which was pushed aside by the mass ejection.

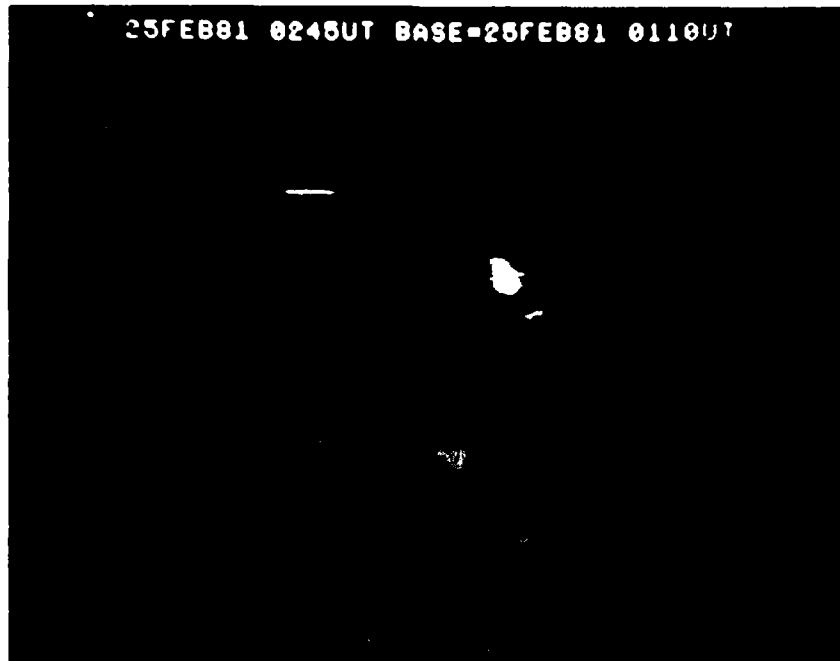


FIGURE 4. A white-light difference image of the coronal mass ejection of 1981 February 23, 0245 UT, observed with the SOLWIND coronagraph. The base image used for differencing was taken at 0110 UT. The field of view of the image extends from the outer edge of the occulting disk, at about $2.6 R_{\odot}$, to $8 R_{\odot}$.

The isodensity contour plot (Figure 5) and radial-cut plot (Figure 6) both show a density profile similar to those of the events studied by JH: a broad ledge of material at the $6 - 56 \times 10^{-9} \text{ g cm}^{-2}$ level extends around the front and sides of the denser ejected material.

The majority of events studied have density distributions similar to that of the February 25 CME and, thus, ostensibly consistent with the results of JH. However, we must consider the following questions in order to determine whether or not this density distribution necessarily indicates preflare (or pre-CME) activity.

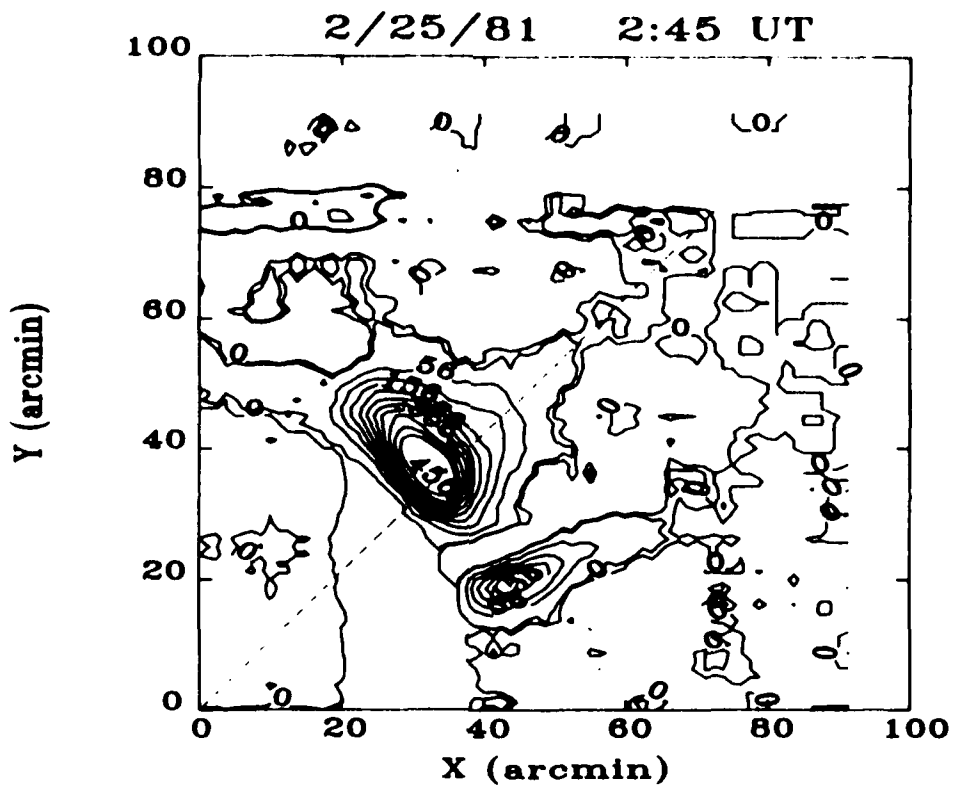


FIGURE 5. Same as Figure 2 for the 1981 February 25 event at 0245 UT, taken from a portion of the image shown in Figure 4.

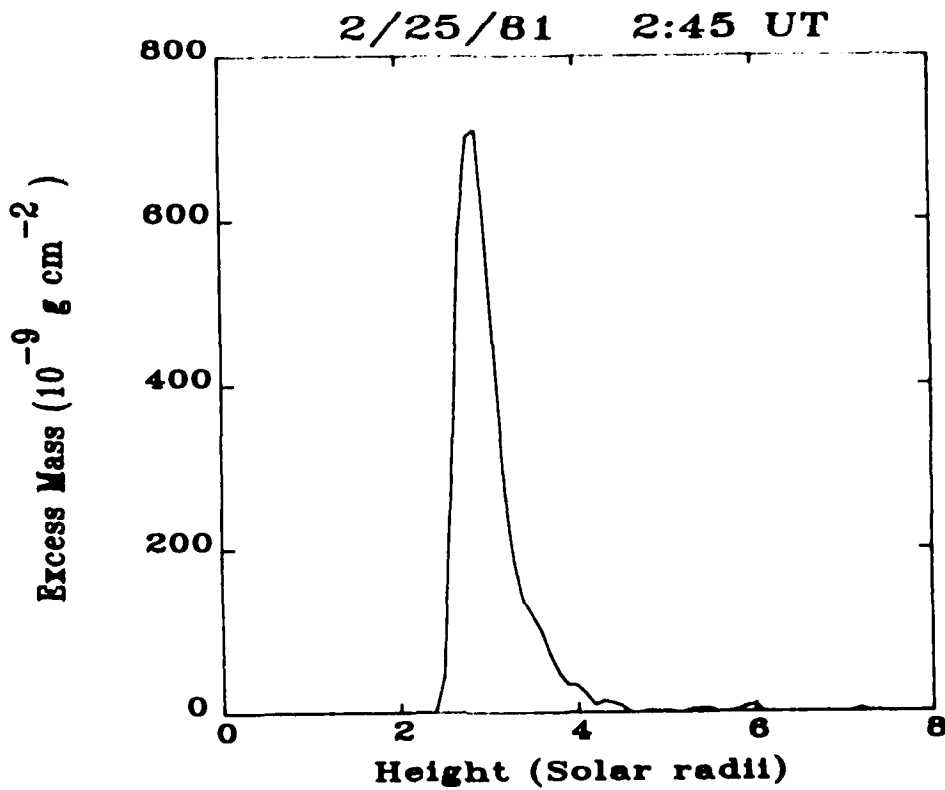


FIGURE 6. Same as Figure 3 for the 1981 February 25 event at 0245 UT, for the radial cut partially shown in Figure 5.

- 1) What is the location of the front of the CME, as determined from the difference images, relative to the column density levels shown in the relevant contour plots? By definition, the material comprising the forerunner must lie ahead of the main body of the CME (as defined through visual determination of the front).
- 2) Is this material associated exclusively with CMEs, or do other coronal phenomena exhibit the same type of density distribution?

For all but a few of the CMEs investigated in this work, visual inspection of the difference images yields positions for the CME fronts that coincide roughly with the $6 \times 10^{-9} \text{ g cm}^{-2}$ level of excess density in the contour plots (compare Figures 1 and 2, or 4 and 5). In other words, this level is plainly visible in all cases where the images are of reasonable quality, i.e., the image is free of a high background level or data drops. Therefore, the images themselves provide no a priori reason to attribute special characteristics to the CME plasma at densities between 6 and $56 \times 10^{-9} \text{ g cm}^{-2}$.

To answer the second question, we return to the 25 February event. Note that the activated streamer exhibits a density profile much like that of the nearby CME, with its own "forerunner"-like plateau (see Figure 5). In fact, if we compare the CME difference images with the contour plots, we find many examples of coronal streamers that are visible at or above the $6 \times 10^{-9} \text{ g cm}^{-2}$ excess-density level. The fact that these streamers are observed in the difference images indicates that the coronal structure has changed since the base image was obtained, either through the introduction of additional mass into preexisting structures or through movement of the streamer itself (as for the 25 February event). These two situations are easily

distinguishable because, in the latter case only, a "depletion" will appear in the difference image at the original location of the affected material (see Figure 4). In either case, these features are not CMEs and there is no reason to expect their density distributions to resemble that of a CME with a forerunner ahead of it. In situations where the CME and the streamer appear cospatial in the plane-of-the-sky images, the contours associated with the excess mass along the streamer would remain stationary, whereas the contours associated with the CME would move outward. The resultant series of contour plots thus would be inconsistent with the definition of a forerunner according to JH.

IV. DISCUSSION

For coronal streamers, the density profile derived from white-light coronagraph observations appears to be a Gaussian perpendicular to the major axis and a power law of the form r^{-n} , where $n \sim 3.8$, along the radial distance r from the solar surface (e.g., Bohlin, Koomen, and Tousey 1971; Saito 1972). Pressure balance arguments (either gravitational or magnetic) also yield power-law density profiles for coronal features. A contour plot of the density distribution in coronal structures should reflect the form of the distribution; if not, misleading inferences can be obtained. We conclude, therefore, that the apparent plateau of low-density material which JH identified as precursor activity can be explained by consideration of the display techniques -- specifically, the choice of contouring levels. The levels chosen by JH (and duplicated in our study) are linearly spaced. If the contour plots are drawn with levels spaced in a different manner -- according to a power law or a Gaussian, for example -- the low-density ledge disappears,

for most events. To illustrate this contention, we have replotted the 25 February event with density levels spaced by powers of 3 (Figure 7).

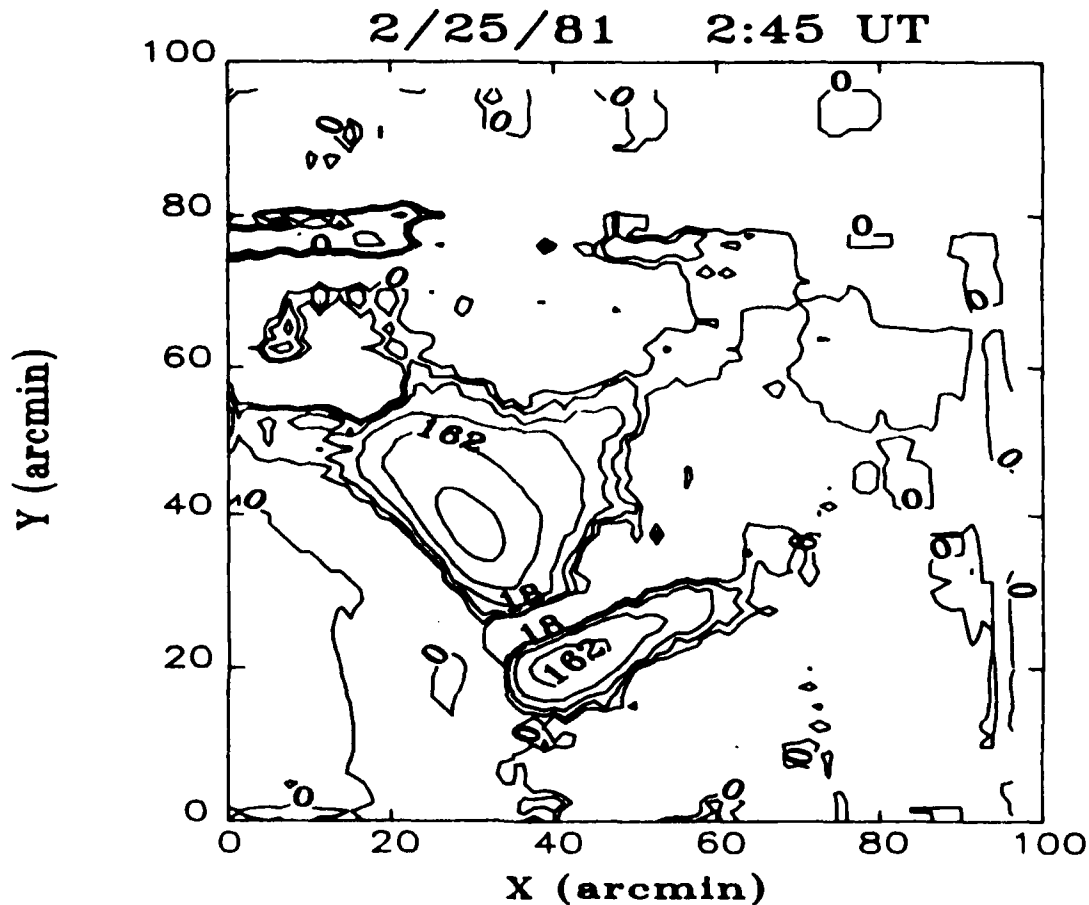


FIGURE 7. Isodensity contours of excess column density (in g cm^{-2}) for the 1981 February 25 event at 0245 UT taken from a portion of the image shown in Figure 1. The contour levels are at 0, 6, 18, 54, 162, and $486 \times 10^{-9} \text{ g cm}^{-2}$ (i.e., 6×3^n). Values above $486 \times 10^{-9} \text{ g cm}^{-2}$ are not shown.

This form was chosen for general consistency with the streamer density profiles derived by Saito (1972), but does not necessarily reflect the true density distribution in the CME. Although fewer contours are shown, it is clear that this plot differs significantly from Figure 5: the contours are more evenly spaced (particularly in the displaced streamer), and there is no

sign of a frontal plateau.

Based on these results, we conclude that the forerunner phenomenon is an artifact of the data-display procedures and does not reflect a genuine pre-CME coronal disturbance. The plateau-like morphology of the lowest-density contour, for linearly spaced levels, can be explained by a combination of the nonlinear density profile and the existence of "background" coronal structures which presumably are activated in conjunction with the CME. This explanation appears satisfactory for all of the events analyzed in the present work -- over twice as many events as were studied by JH. Of course, we cannot rule out the existence of forerunner activity at a level below $6 \times 10^{-9} \text{ g cm}^{-2}$, or with a thickness smaller than the SOLWIND spatial resolution.

The difference between SKYLAB and SOLWIND techniques for data collecting and reduction might be partially responsible for the contradictory results. For the SOLWIND data, we can compare directly the images and the contour plots constructed from the same digital data for each CME. The SKYLAB images, on the other hand, were obtained on film (a well-known nonlinear medium), while the contour plots were produced by digitization of the film images.

Searches for forerunners in other coronagraph data sets would be very useful to resolve this discrepancy between the SKYLAB and SOLWIND results. At present, the Coronagraph/Polarimeter on board the SMM satellite is the only other spaceborne instrument which has observed a significant number of CMEs during the present solar cycle. We suggest that such a search should be repeated when future experiments have collected a sufficiently large sample of bright, well-defined CMEs of the appropriate morphological types. In addition, because the SOLWIND data is still being reduced, we intend to

continue our investigation as new CMEs are discovered. Two unresolved questions which we will address in our extended investigation are focussed on the underlying physics of CMEs and potential sources of low-visibility density enhancement ahead of the main body of the mass ejection:

- 1) If a shock is driven ahead of the leading edge of a CME, could it be detected in the SOLWIND data and what would be its signature?
- 2) What causes coronal streamers to be pushed aside by CMEs? If the causative agent is a pressure wave, would that wave be detectable in the SOLWIND data?

ACKNOWLEDGEMENTS

This research was supported in part by the Air Force Geophysics Laboratory, through MIPR FY71218500006. I wish to thank Russell A. Howard for patiently instructing me how to calibrate, convert, and display the SOLWIND data, and for invaluable discussions on the results and interpretation of the present study .

REFERENCES

- Bird, M.K., Volland, H., Howard, R.A., Koomen, M.J., Michels, D.J., Sheeley, N.R., Jr., Armstrong, J.W., Seidel, B.L., Stelzreid, C.T., and Woo, R. 1985, *Solar Phys.*, 98, 341.
- Bohlin, J.D., Koomen, M.J., and Tousey, R. 1971, *Solar Phys.*, 21, 408.
- Dulk, G.A., Smerd, S.F., MacQueen, R.M., Gosling, J.T., Magun, A., Stewart, R.T., Sheridan, K.V., Robinson, R.D., and Jacques, S. 1976, *Solar Phys.*, 49, 369.
- Gary, D.E., Dulk, G.A., House, L.L., Illing, R., Sawyer, C., Wagner, W.J., McLean, D.J., and Hildner, E. 1984, *Astr. Ap.*, 134, 122.
- Gergely, T.E. 1984, in *Proc. STIP Symposium on Solar/Interplanetary Intervals*, eds. M.A. Shea, D.F. Smart, and S.M.P. MacKenna-Lawlor (Huntsville: Engineering International, Inc.), p. 237.
- Gosling, J.T., Hildner, E., MacQueen, R.M., Munro, R.H., Poland, A.I., and Ross, C.L. 1974, *J.G.R.*, 79, 4581.

- Harrison, R.A., Waggett, P.W., Bentley, R.D., Phillips, K.J.H., Bruner, M., Dryer, M., and Simnett, G.M. 1985, *Solar Phys.*, 97, 387.
- Hildner, E. 1977, in *Study of Travelling Interplanetary Phenomena*, eds. M.A. Shea, D. Smart, and S.T. Wu (Dordrecht: Reidel), p. 3.
- Hildner, E., Gosling, J.T., Hansen, R.T., and Bohlin, J.D. 1975, *Solar Phys.*, 45, 363.
- Howard, R.A., Sheeley, Jr., N.R., Koomen, M.J., and Michels, D.J. 1985, *J.G.R.*, 90, 8173.
- Jackson, B.V., and Hildner, E. 1978, *Solar Phys.*, 60, 155.
- Jackson, B.V. 1981, *Solar Phys.*, 73, 133.
- Koomen, M.J., Howard, R., Hansen, R., and Hansen, S. 1974, *Solar Phys.*, 34, 447.
- Lee, J.S. 1981, *Computer Graphics Image Processing*, 15, 380.
- Low, B.C. 1981, *Ap. J.*, 251, 352.
- Low, B.C. 1982, *Ap. J.*, 254, 796.
- Low, B.C. 1984, *Ap. J.*, 281, 392.
- MacQueen, R.M. 1980, *Phil. Trans. R. Soc. London A*, 297, 605.
- Malitson, H.H., Fainberg, J., Stone, R.G. 1973, *Ap. J.*, 183, 111.
- Michels, D.J., Howard, R.A., Koomen, M.J., and Sheeley, Jr., N.R. 1980, in *Radio Physics of the Sun*, eds. M.R. Kundu and T.E. Gergely (Dordrecht: Reidel), p. 439.
- Michels, D.J., Sheeley, Jr., N.R., Howard, R.A., and Koomen, M.J. 1982, *Science*, 215, 1097.
- Mouschovias, T. Ch., and Poland, A.I. 1978, *Ap. J.*, 220, 675.
- Munro, R.H., Gosling, J.T., Hildner, E., MacQueen, R.M., Poland, A.I., and Ross, C.L. 1979, *Solar Phys.*, 45, 377.
- Munro, R.H., and Sime, D. 1985, *Solar Phys.*, 97, 191.
- Poland, A.I., Howard, R.A., Koomen, M.J., Michels, D.J., and Sheeley, N.R., Jr. 1981, *Solar Phys.*, 69, 169.
- Saito, K. 1972, *Annals of the Tokyo Astronomical Observatory (Second Series)*, 13, 93.
- Sheeley, Jr., N.R., Howard, R.A., Michels, D.J., and Koomen, M.J. 1980, *Ap. J. (Letters)*, 237, L99.

Sheeley, N.R., Jr., Howard, R.A., Koomen, M.J., Michels, D.J., Schwenn, R.,
Mulhauser, K.H., and Rosenbauer, H. 1983, Solar Wind Five, NASA Conf.
Publ. 2280, p. 693.

Sheeley, N.R., Jr., Howard, R.A., Koomen, M.J., Michels, D.J., Schwenn, R.,
Mulhauser, K.H., and Rosenbauer, H. 1985, J.G.R., 90, 163.

Simnett, G.M., and Harrison, R.A. 1985, Solar Phys., 99, 291.

Wild, J.P., Smerd, S.F., and Weiss, A.A. 1963, Ann. Rev. Astr. Ap., 1, 291.

Wolfson, R., and Gould, S.A. 1985, Ap. J., 296, 287.

Woo, R., Armstrong, J.W., Sheeley, N.R., Jr., Howard, R.A., Koomen, M.J.,
Michels, D.J., and Schwenn, R. 1985, J.G.R., 90, 154.

Wu, S.T., Dryer, M., Nakagawa, Y., and Han, S.M. 1978, Ap. J., 219, 324.

END

DTIC

9-86